
OPTICS AND SPECTROSCOPY.
LASER PHYSICS

Attosecond Interferometry of Neon Atom: Photoelectron Angular Distributions

S. N. Yudin^{1*}, M. M. Popova^{1,2}, M. D. Kiselev^{1,2,3},
S. M. Burkov³, E. V. Gryzlova¹, and A. N. Grum-Grzhimailo¹

¹*Skobeltsyn Institute of Nuclear Physics, Lomonosov Moscow State University, Moscow, 119234 Russia*

²*Faculty of Physics, Lomonosov Moscow State University, Moscow, 119234 Russia*

³*Laboratory for Modeling of Quantum Processes, Pacific National University, Khabarovsk, 680035 Russia*

Received February 10, 2023; revised March 2, 2023; accepted March 7, 2023

Abstract—In the paper we present the angular distributions of photoelectrons in ionization of neon atom by a field of several multiple frequencies. The considered setup is referred to the RABBITT (reconstruction of attosecond beating by interference of two-photon transitions) spectroscopy under condition that the field frequencies are selected in such a way that resonant transitions through discrete states play an important role. The role of the phase of the seeding infrared field on the angular distributions of photoemission is analyzed. A significant difference in the anisotropy parameters at the near-threshold sideband caused by transitions through discrete states is shown. Two methods are compared: numerical solution of the rate equations with continuum discretization and third-order perturbation theory.

Keywords: attosecond beams, RABBITT spectroscopy, harmonic generation, phase control, multiphoton ionization, photoelectron angular distributions, transition matrix elements, photoionization amplitude, R-matrix

DOI: 10.3103/S0027134923030220

INTRODUCTION

The creation of intense sources of ultrashort radiation pulses in the vacuum ultraviolet (VUV) and X-ray ranges based on the high harmonic generation (HHG) method [1–3] has made possible experimental studying the dynamics of small quantum systems on attosecond timescales [4–8]. One of the methods used to study the dynamics of electrons in atoms, molecules, and solids is RABBITT spectroscopy (reconstruction of attosecond beating by interference of two-photon transitions) [9].

The method is based on irradiating of a target by a combined electromagnetic field consisting of a strong infrared (IR) pulse and several its high-order harmonics in the VUV range. The absorption of a high-frequency photon promotes an electron into continuum (see Fig. 1)—*the main line* (ML), and the subsequent absorption or emission of an IR photon, which is possible in the Coulomb field of the ion may promote it into *sidebands* (SB) [10]. Variation of the IR pulse delay time τ with respect to the VUV leads to the appearance of characteristic oscillations

in the photoelectron spectra and allows for control of the resulting photoelectron characteristics and obtaining information about the relative phases of the transition amplitudes [11].

At the very beginning both experimental and theoretical studies of RABBITT spectroscopy were devoted to integrated over the electron emission angle quantities [12–14]. Recently, angle-resolved RABBITT measurements have been performed [15–20]. The corresponding calculations were carried out for noble gas atoms [16, 21–24]. Of particular interest are the angle-resolved RABBITT studies carried out in a vicinity of a resonance [25]. General tendencies can be effectively tracked using analytical methods [26–30].

In the present paper we develop the theoretical study of the features of neon RABBITT spectroscopy initiated in [31], where photoelectron spectra, amplitude and phase of RABBITT oscillations were obtained, and the influence of the intensity of the seeding IR field and detuning from the resonance upon excitation of discrete states was studied. Similar to [31], we use two different approaches to obtain the angular

*E-mail: yudinsn@gmail.com

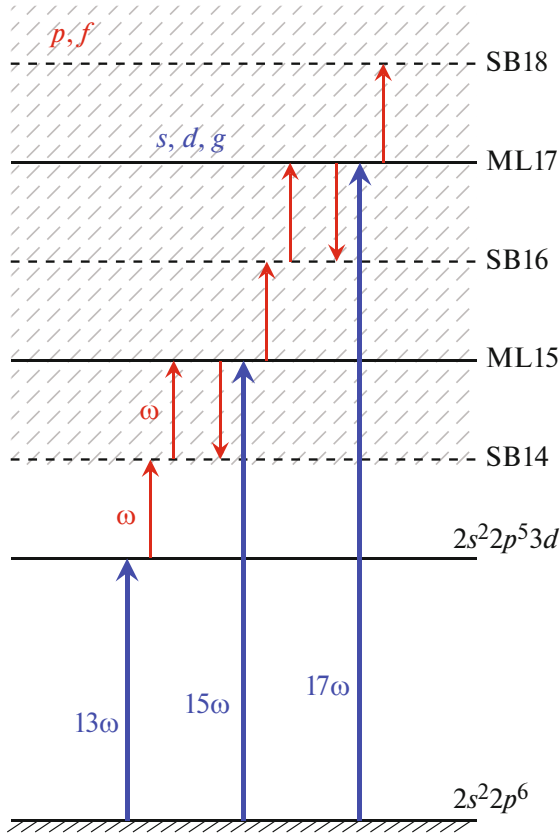


Fig. 1. The scheme of multifrequency ionization of Ne at wavelength of the IR seeding harmonic $\lambda = 800$ nm and its 13th, 15th, and 17th VUV harmonics.

distributions of photoelectrons: solution of rate equations and perturbation theory. The results of both approaches are analyzed and compared with each other. Transition matrix elements between different states of the discrete spectrum as well as between states of the discrete spectrum and continuum were obtained by the stationary R-matrix method [32]; to describe the transitions between continuum states, the divergence elimination method [33, 34] was applied with single-electron wave functions obtained by [35].

Unless otherwise specified, the atomic system of units is used.

1. THE BASEMENT OF THE METHODS

The detailed description of the applied methods, i.e., the numerical solution of the system of rate equations (SRE) and the nonstationary perturbation theory (PT), as well as a description of the spectroscopic model, is presented in [31]. Here we provide only the milestones of the methods.

A wave function $\Psi(\mathbf{r}, t)$ of the system exposed to an electromagnetic field with the vector potential

$A(t)$, which in the RABBITT experiments is the sum of an IR pulse and several its N th order harmonics in the VUV range, expands in eigenfunctions $\phi_n(\mathbf{r})$ of the unperturbed (atomic) Hamiltonian \hat{H}_{at} . The resulting system of first-order differential equations for the expansion coefficients $a(t)$ which determine the evolution of the population of atomic states

$$\frac{da_f(t)}{dt} = -i \sum_i e^{i(\varepsilon_f - \varepsilon_i)t} \frac{1}{c} \langle \phi_f | A(t) \mathbf{p} | \phi_i \rangle a_i(t) \quad (1)$$

is solved numerically in the SRE method using the original program [37] with the initial condition that the system is in the ground state in the beginning of the electromagnetic field; here the indices i and f of the expansion coefficients denote all quantum numbers defining the state, ε is the energy of the state, \mathbf{p} is the momentum operator. The discretization method was used to describe the states of the continuum.

For the nonstationary PT, the coefficients $a_f(t)$ in the Eq. (1) are expanded into a series further:

$$a_f(t) = a_f^{(0)}(t) + a_f^{(1)}(t) + a_f^{(2)}(t) + \dots, \quad (2)$$

here $a_f^{(0)}(t) = \delta_{fi}$ is solution without perturbation.

In perturbation theory, the first order $a_f^{(1)}(t)$ describes one-photon transitions from the ground state to excited discrete states and into the continuum in the region of the main lines ML, which occur due to the absorption of the VUV photon ω_N , the second order $a_f^{(2)}(t)$ —transitions from the excited states and from the main lines to the sidebands SB, caused by the absorption or emission of an infrared photon ω_{ir} , finally, the third order $a_f^{(3)}(t)$ and its interference with $a_f^{(1)}(t)$ describe transitions with absorption and/or emission of two infrared photons.

The main qualitative difference between SRE and PT is that the second method does not take into account strong field effects such as the Stark shift and multiphoton absorption. In addition, in perturbation theory, there is no depletion of the states population caused by subsequent transitions, that means that the total population is not conserved.

Typically in RABBITT experiments, both IR and VUV components are linearly polarized. The photoelectron angular distribution after the pulse for linearly polarized fields in the jK -coupling representation, which is necessary for describing photoelectron spectra near the threshold, is given by [38]:

$$\begin{aligned}
 W(\varepsilon, \theta) = \frac{1}{4\pi} \sum_{JJ'KK'l'l'k} (-1)^{J_f - \frac{1}{2}} \hat{K} \hat{K}' \hat{J} \hat{J}' \hat{l} \hat{l}' (l0, l'0 | k0) (J0, J'0 | k0) \begin{Bmatrix} k & l & l' \\ J_f & K' & K \end{Bmatrix} \begin{Bmatrix} k & J & J' \\ \frac{1}{2} & K' & K \end{Bmatrix} \\
 \times a_f a_{f'}^* i^{l'-l} \exp(i(\sigma_l + \delta_l - \sigma_{l'} - \delta_{l'})) P_k(\cos \theta), \quad (3)
 \end{aligned}$$

where $P_k(\cos \theta)$ are the Legendre polynomials of the k th order, the angle θ is counted from the direction of the polarization vector; the construct in curly braces is the $6j$ Wigner symbol; δ_l and σ_l are the Coulomb phase and scattering phase of the partial channel l ; l and l' are the orbital momentum of the electron, J_f is the total moment of the residual ion, K and K' are the sum of the momentum of the ion and electron. Let us emphasize that the angular distribution (3) is axially symmetric with respect to the polarization vector.

The PAD can be presented in a conventional form:

$$\begin{aligned}
 W(\varepsilon, \theta) = \frac{\sigma(\varepsilon)}{4\pi} (1 + \beta_2(\varepsilon) P_2(\cos \theta) \\
 + \beta_4(\varepsilon) P_4(\cos \theta)), \quad (4)
 \end{aligned}$$

which is the definition of the angular anisotropy parameters β_2 and β_4 ; $\sigma(\varepsilon)$ is the probability of electron photoemission with energy ε .

2. RESULTS AND DISCUSSION

We assume that the electromagnetic field is linearly polarized along the quantization axis with an electric strength in the form:

$$\begin{aligned}
 E(t) = \sum_N \cos^2(t/\sigma_N) E_N \cos(\omega_N t + \phi_N) \\
 + E_{\text{ir}} \cos^2(t/\sigma_{\text{ir}}) \cos(\omega_{\text{ir}} t + \phi_{\text{ir}}). \quad (5)
 \end{aligned}$$

The cosine half-period was used as an envelope, since it possesses the necessary smoothness conditions for the field and its first derivative at the beginning and the end of the pulse. Additionally it may be integrated analytically, in contrast to the field with the Gaussian envelope.

In this paper, we assume the typical values of electromagnetic radiation parameters implemented on the HHG facilities: IR pulse of 800 nm with maximum intensity of $E_{\text{ir}} = 25.7 \times 10^6$ V/cm (5×10^{-3} au) and width (duration) at half amplitude $\sigma_{\text{ir}} = 20\sqrt{2}$ fs and VUV pulse containing $N = 11, 13, 15, 17, 19$ harmonics with duration two times less and intensity 50 times less. Note that the width of the Gaussian pulse with the same behavior at the maximum is 20 fs. With such a width the pulse contains about 30 optical cycles. For pulses containing a

large number of optical cycles, changing the pulse delay is equivalent to changing the phase of the IR field $\phi_{\text{ir}} = \omega_{\text{ir}} \tau$ with respect to the VUV. At this wavelength, the 13th harmonic is close to resonant excitation of the $2p^5(^2P_{1/2})3d[3/2]_1$ state.

Following the methods described in section 1, we obtained the expansion coefficients a_f after the pulse and the anisotropy parameters $\beta_{2,4}$ which are shown in Figs. 2b and 2c. The dots show the results obtained by the SRE method, shifted for convenience of comparison by 0.05 eV to the right in the photoelectron energy in order to eliminate the Stark shift effect (see [31]), and the solid lines mark PT. The bright color indicates the values averaged over the phase of the infrared field, and the light color indicates their maximum and minimum values. The black color marks the averaged spectrum of photoelectrons (Fig. 2a). The angular anisotropy parameters periodically change as the coefficients at each Legendre polynomial in (3) oscillate at twice the frequency of the IR field. However, the dimensionless parameters in (4) are not harmonic functions. Since the angular anisotropy parameters are the ratio of a some quantity to the cross section, at energies for which the probability of electron emission is below the limit of numerical accuracy, the anisotropy parameters experience sharp fluctuations that have no physical meaning, and therefore are not presented.

Transitions to the main lines occur with the absorption or emission of an odd number of photons, and the parity of such states is opposite to the parity of the ground state, while transitions to the sidebands require an even number of photons. Upon ionization of the neon valence shell ($2p$)—the target under consideration—this leads to even orbital angular momenta in ML (s, d, g), and odd—in SB (p, f) (see Fig. 1), that explains the difference in the $\beta_{2,4}$ values of the mainlines and sidebands.

It should be noted that for the mainlines and SB14 the cross section is always nonzero, while for the sidebands SB16,18 there is a phase of the infrared field at which it tends to zero. This explains the discrepancy between the two approaches observed at some energies in the maximum value of $\beta_{2,4}$ in SB16,18 with the same averaged values.

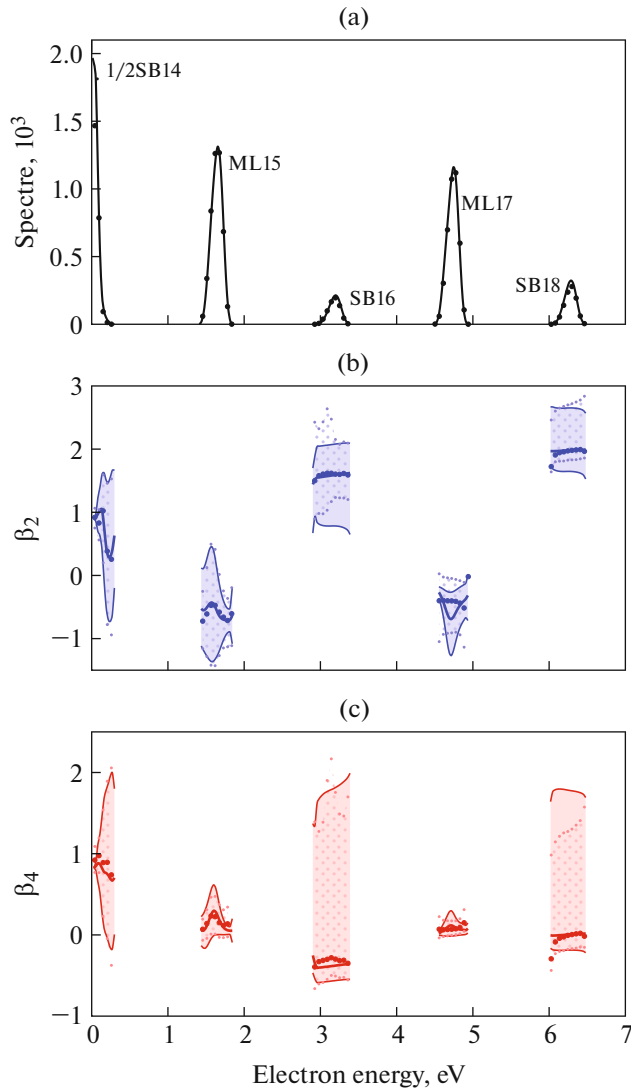


Fig. 2. Spectrum averaged over IR field phase (a), photoelectron angular anisotropy parameter β_2 (b) and β_4 (c), obtained by the SRE method (points) and PT (lines); thin lines and light dots bordering the shaded areas in panels (b) and (c) mark the domain of parameter change for the corresponding method.

The parameter β_2 at photoelectron energies corresponding to ML can be very different from observed in conventional single-photon ionization [39], which indicates a large contribution to the formation of anisotropy of the third-order amplitudes in PT, which do not make a noticeable contribution to the integral cross-section. The β_4 parameter in ML arises only due to the presence of the third-order amplitudes with total moment $J = 3$.

Figure 3 shows the shape of the angular distribution of photoelectron emission at a fixed photoelectron energy corresponding to the probability maxima in SB14, ML15, SB16, and ML17 for three phases of the seeding field. It can be seen that the angular dis-

tributions in the SB14 and ML15 are slightly different in different approaches. The difference in SB16 and ML17 is more significant. This difference is explained by the fact that although the maximum and minimum values of the angular anisotropy parameters in the SRE and PT coincide, they are achieved at slightly different phases of the IR field. Under the real experiment conditions, when natural averaging over an interval of the IR field phase and the photoelectron energy takes place, the angular distributions will coincide. The most significant difference in the angular distributions observed for SB16 at $\phi_{\text{ir}} = \pi/2$ (red lines in Fig. 3c) is explained by the fact that the probability of photoemission at these parameters is almost zero.

We would like to emphasize that SB14 is partly formed by transitions through discrete states of the $2p^53d$ configuration excited via the absorption of a photon of the 13th harmonic by $2p$ -electron which leads to a significant difference between this part of the spectrum and the higher-energy region. The predicted SRE and PT variations angular anisotropy parameters in SB14 depending on the ϕ_{ir} are in better agreement with each other than the variation of the integrated spectra in this region [31]. The weak dependence of the angular distributions on the phase in SB14 (Fig. 3a) indicates the dominance of one of the transition paths in this region, namely the resonant transition through $2p^53d$ discrete states with absorption $13\omega_{\text{ir}}$ and subsequent ionization by ω_{ir} into a state with $l = 3$. The unusual phase dependence of ML15 (Fig. 3b) is caused, in turn, by the dominance of transitions from $l = 3$ with ω_{ir} absorption.

CONCLUSIONS

The paper presents the results of calculations of the angular distributions of photoelectrons emitted from neon atom in the field of several harmonics of the driving infrared field. The difference in the shape of the angular distributions for the mainlines and sidebands is demonstrated and explained. The influence of transitions through states of the discrete spectrum is analyzed.

Angular distributions provide more detailed information on the relative phases of harmonics than integral spectra, since the contribution of channels with higher momentum is more essential. For example, for emission from the valence $2p$ -shell of neon atom, these are contributions of continuum channels with orbital momentum $l = 4$ (g -waves).

It is shown that while the solution of the rate equations system and perturbation theory give the same results for the angle-integrated probability even for the lower not adjacent to the threshold lines (starting from SB16, see [31]), the agreement in the angular

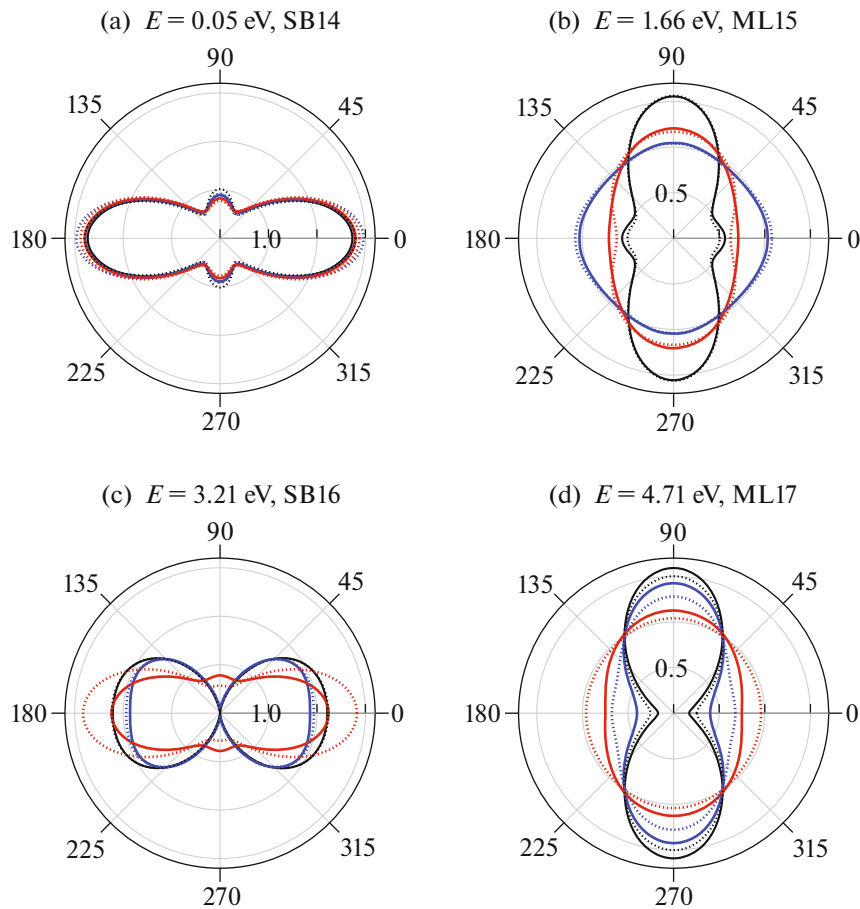


Fig. 3. The sections of the photoelectron angular distribution by a plane passing through the symmetry axis for three phases of the infrared field $\phi_{\text{ir}} = 0$ —black line, $\phi_{\text{ir}} = \pi/4$ —blue, $\phi_{\text{ir}} = \pi/2$ —red; solid lines show PT results, dotted lines—SRE. The angular distributions are dimensionless quantities, the scale for SB (a, c) and for ML (b, d) differ by a factor of two.

distributions is slightly worse. This happens because the considered angular distributions are, in fact, triply differential: over the emission angle and energy of the photoelectron, and over the phase of the infrared field. Provided that the probability is reduced to a doubly differential one, i.e., either averaging over the phase of the IR field or integrating over the angle of emission of a photoelectron, agreement is restored.

This study is an important step towards extension the theory of RABBITT spectroscopy to systems with nonconventional geometries, since for many of them (for example, for circularly polarized harmonics), RABBITT oscillations appear only in differential characteristics.

FUNDING

The research was funded by the Russian Foundation for Basic Research under project no. 20-52-12023, by Ministry of Science and Higher Education of the Russian Federation grant no. 075-15-2021-1353 and by the Ministry of Science and Higher Ed-

ucation of the Russian Federation (project no. 0818-2020-0005) using resources of the Shared Services “Data Center of the Far-Eastern Branch of the Russian Academy of Sciences.”

CONFLICT OF INTEREST

The authors declare that they have no conflicts of interest.

REFERENCES

1. M. Lewenstein, Ph. Balcou, M. Yu. Ivanov, et al., *Phys. Rev. A* **49**, 2117 (1994).
<https://doi.org/10.1103/PhysRevA.49.2117>
2. G. Sansone, E. Benedetti, F. Calegari, et al., *Science* **314**, 443 (2006).
<https://doi.org/10.1126/science.1132838>
3. V. V. Strelkov, V. T. Platonenko, A. F. Sterzhantov, and M. Yu. Ryabikin, *Phys. Usp.* **59**, 425 (2016).
<https://doi.org/10.3367/UFNe.2015.12.037670>
4. F. Krausz and M. Ivanov, *Rev. Mod. Phys.* **81**, 163 (2009).
<https://doi.org/10.1103/RevModPhys.81.163>

5. P. M. Paul, E. S. Toma, P. Breger, et al., *Science* **292**, 1689 (2001).
<https://doi.org/10.1126/science.1059413>
6. R. Pazourek, S. Nagele, and J. Burgdörfer, *Faraday Discuss* **163**, 353 (2013).
<https://doi.org/10.1039/c3fd00004d>
7. J. Vos, L. Cattaneo, S. Patchkovskii, et al., *Science* **360**, 1326 (2018).
<https://doi.org/10.1126/science.aao4731>
8. M. Ossiander, J. Riemensberger, S. Neppl, et al., *Nature* **361**, 374 (2018).
<https://doi.org/10.1038/s41586-018-0503-6>
9. V. Vénier, R. Taïeb, and A. Maquet, *Phys. Rev. A* **54**, 721 (1996).
<https://doi.org/10.1103/PhysRevA.54.721>
10. N. B. Deloene and V. P. Krainov, *Nonlinear Ionization of Atoms by Laser Radiation* (Fizmatlit, Moscow, 2001).
11. M. Swoboda, T. Fordell, K. Klünder, et al., *Phys. Rev. Lett.* **103**, 103003 (2010).
<https://doi.org/10.1103/PhysRevLett.104.103003>
12. K. Klünder, J. M. Dahlström, M. Gisselbrecht, et al., *Phys. Rev. Lett.* **106**, 143002 (2011).
<https://doi.org/10.1103/PhysRevLett.106.143002>
13. D. Guénot, D. Kroon, E. Balogh, et al., *J. Phys. B* **47**, 245602 (2014).
<https://doi.org/10.1088/0953-4075/47/24/245602>
14. M. Sabbar, S. Heuser, R. Boge, et al., *Phys. Rev. Lett.* **115**, 133001 (2015).
<https://doi.org/10.1103/PhysRevLett.115.133001>
15. S. Heuser, A. Jiménez Galán, C. Cirelli, et al., *Phys. Rev. A* **94**, 063409 (2016).
<https://doi.org/10.1103/PhysRevA.94.063409>
16. P. Hockett, *J. Phys. B* **50**, 154002 (2017).
<https://doi.org/10.1088/1361-6455/aa7887>
17. D. Busto, J. Vinbladh, S. Zhong, et al., *Phys. Rev. Lett.* **123**, 133201 (2019).
<https://doi.org/10.1103/PhysRevLett.123.133201>
18. J. Fuchs, N. Douguet, S. Donsa, et al., *Optica* **7**, 154 (2020).
<https://doi.org/10.1364/OPTICA.378639>
19. D. Bharti, D. Atri-Schuller, G. Menning, et al., *Phys. Rev. A* **103**, 022834 (2021).
<https://doi.org/10.1103/PhysRevA.103.022834>
20. J. Peschel, D. Busto, M. Plach, et al., *Nature Commun.* **13**, 5205 (2022).
<https://doi.org/10.5878/h5yr-gb56>
21. J. M. Dahlström and E. Lindroth, *J. Phys. B* **47**, 124012 (2014).
<https://doi.org/10.1088/0953-4075/49/20/209501>
22. J. Wätzel, A. S. Moskalenko, Y. Pavlyukh, and J. Berakdar, *J. Phys. B* **48**, 025602 (2014).
<https://doi.org/10.1088/0953-4075/48/2/025602>
23. I. A. Ivanov and A. S. Kheifets, *Phys. Rev. A* **96**, 013408 (2017).
<https://doi.org/10.1103/PhysRevA.96.013408>
24. A. W. Bray, F. Naseem, and A. S. Kheifets, *Phys. Rev. A* **97**, 063404 (2018).
<https://doi.org/10.1103/PhysRevA.97.063404>
25. C. Cirelli, C. Marante, and S. Heuser, *Nat. Commun.* **9**, 955 (2018).
<https://doi.org/10.1038/s41467-018-03009-1>
26. M. V. Frolov, N. L. Manakov, T. S. Sarantseva, et al., *Phys. Rev. Lett.* **102**, 243901 (2009).
<https://doi.org/10.1103/PhysRevLett.102.243901>
27. M. V. Frolov, N. L. Manakov, A. M. Popov, et al., *Phys. Rev. A* **85**, 033416 (2012).
<https://doi.org/10.1103/PhysRevA.85.033416>
28. A. Galstyan, Y. V. Popov, F. Mota-Furtado, et al., *Eur. Phys. J. D* **71**, 97 (2017).
<https://doi.org/10.1140/epjd/e2017-70707-8>
29. B. Ghomashi, N. Douguet, and L. Argenti, *Phys. Rev. A* **99**, 053407 (2019).
<https://doi.org/10.1103/PhysRevA.99.053407>
30. V. A. Astapenko, *JETP* **162**, 1(7), 5 (2022).
<https://doi.org/10.31857/S0044451022060000>
31. M. M. Popova, S. N. Yudin, M. D. Kiselev, et al., *JETP* **136** (3), 250 (2023).
<https://doi.org/10.31857/S004445102303001X>
32. O. Zatsarinny, *Comput. Phys. Commun.* **174**, 273 (2006).
<https://doi.org/10.1016/j.cpc.2005.10.006>
33. T. Mercouris, Y. Komninos, S. Dionissopoulou, and C. A. Nicolaides, *J. Phys. B* **29**, 13 (1996).
<https://dx.doi.org/10.1088/0953-4075/29/1/004>
34. S. A. Novikov and A. N. Hopersky, *J. Phys. B* **44**, 235001 (2011).
<https://doi.org/10.1088/0953-4075/44/23/235001>
35. C. F. Fischer, T. Brage, and P. Jonsson, *Computational Atomic Structure: An MCHF Approach* (IOP Publishing, Bristol, 1997).
36. D. A. 36, A. N. Moskalov, and V. K. Khersonskii, *Quantum Theory of Angular Momentum* (World Scientific, Singapore, 1988).
37. S. N. Yudin, S. M. Burkov, A. N. Grum-Grzhimajlo, M. D. Kiselev, and V. I. Severinenko, RF State registration certificate no. 2021681060 (December 17, 2021).
38. V. V. Balashov, A. N. Grum-Grzhimailo, and N. M. Kabachnik, *Polarization and Correlation Phenomena in Atomic Collisions: A Practical Theory Course* (Kluwer Academic, New York, 2000).
39. K. Codling, R. G. Houlgatet, J. B. West, and P. R. Woodruff, *J. Phys. B* **9**, 5 (1976).